Journal of Nuclear Materials 408 (2011) 246–256

Contents lists available at ScienceDirect

Journal of Nuclear Materials

journal homepage: www.elsevier.com/locate/jnucmat

Impact of localized deformation on IASCC in austenitic stainless steels

Z. Jiao *, G.S. Was

University of Michigan, Department of Nuclear Engineering and Radiological Sciences, Ann Arbor, MI 48109, United States

ARTICLE INFO

Article history:
Received 1 February 2010
Accepted 7 October 2010
Available online 26 November 2010

ABSTRACT

Localized deformation has been identified as a potential primary contributor to IASCC. Seven austenitic alloys were irradiated to 1 and 5 dpa at 360 °C using 2–3.2 MeV protons and were tested both in simulated BWR environment and in argon. Cracking susceptibility was evaluated at both 1% and 3% strain intervals using crack length per unit area. Stacking fault energy (SFE), hardness, radiation-induced segregation (RIS) and localized deformation were characterized and their correlations with cracking were evaluated using a proposed term, correlation strength. Both SFE and hardness contributed to cracking but neither was the dominant factor. RIS did not play an important role in this study. The correlation strength of localized deformation with IASCC was found to be significantly higher than for others parameters, implying that localized deformation is the most important factor in IASCC. Although not well understood, localized deformation may promote cracking through intensive interaction of dislocations in slip channels with grain boundaries.

1. Introduction

Irradiation-assisted stress corrosion cracking (IASCC) has been a critical problem affecting the cracking of core components in light water reactors (LWRs) since the first IASCC incidents reported in 1960s in 300-series stainless steel fuel rod cladding [1] over 40 years ago. It has occurred in many components such as 304 SS control rod absorber tubes, fuel bundle cap screws, control rod blade handles, sheaths and follower rivets, plate type control blades and instrument dry tubes in BWRs [2]. It has taken on new urgency with the growing interest in extending operating licenses for the current generation of plants to 60 years or beyond in US. What makes IASCC unique is that it is largely controlled by the persistent damage induced by irradiation. That is, while radiation affects the environment through radiolysis, the onset of cracking in LWR environments is controlled by the radiation-induced persistent defects and damage in the alloy [3].

In LWR conditions, the irradiated microstructure is dominated by the formation and evolution of faulted dislocation loops. One of the prime consequences is an increase in the hardness and yield strength and a decrease in uniform elongation [4,5]. Those changes, especially the increase in yield strength, may have adverse effects on cracking of austenitic alloys. For instance, Bruemmer et al. [6] found that there was a threshold of the increase in yield strength (600 MPa), above which IGSCC occurred. Speidel and Magdowski [7] also reported that crack growth rate increased with yield strength in stainless steels in 288 °C BWR water. Since yield strength and hardness are closely related, a similar contribution of hardness to IASCC is also expected.

Radiation-induced segregation (RIS) at grain boundaries is another important factor that is believed to contribute to IASCC. Irradiation causes the depletion of Cr at grain boundaries along with enrichment of Ni and Si. If the grain boundary Cr content falls below a level where a protective Cr_2O_3 film can form, passivation may not be possible and the grain boundary can be more susceptible to corrosion and consequently IASCC.

The stacking fault energy (SFE) is an intrinsic property of the alloy that varies with alloy composition but should not be affected by irradiation. However, the irradiated microstructure may be affected by SFE. For instance, SFE may affect the population and size of faulted dislocation loops since the total energy of the loops includes a portion that is proportional to SFE [8]. SFE also affects dislocation slip behavior in austenitic alloys. Cross-slip is easy in high SFE alloys, but it is difficult in low SFE alloys. Low SFE has been related to IGSCC [3] and is believed to be a potential contributor to IASCC.

In recent years, localized deformation has gained attention as a potential contributor to IASCC. In irradiated alloys, deformation is localized into dislocation channels in which the deformation can be hundreds of times that of the total applied strain. Due to dislocation channeling, deformation of irradiated austenitic alloys is very inhomogeneous. Bruemmer et al. [9] noted that localized deformation can be detrimental to IASCC by promoting dislocation pileups at the grain boundaries. Localized deformation can also lead to localized grain boundary sliding that can rupture the oxide film [3,10] A few studies by the authors [10–13] and others [14,15] also pinpointed localized deformation as a significant contributor to IASCC.

* Corresponding author. Tel.: +1 734 6157761; fax: +1 734 763 4540.
E-mail address: zjiao@umich.edu (Z. Jiao).

0022-3115/$ - see front matter © 2010 Elsevier B.V. All rights reserved.
doi:10.1016/j.jnucmat.2010.10.087

One of the difficulties in determining the mechanism of IASCC is that RIS, loop microstructure, hardening and localized deformation all develop at roughly the same rate and tend to saturate at roughly the same dose. So identifying which irradiated microstructure feature, or combination of features, is responsible for the observed IASCC is extremely difficult. This paper will quantitatively evaluate the correlation of each feature with the observed cracking behavior to determine its relative importance in irradiation-assisted stress corrosion cracking.

2. Experimental

2.1. Sample preparation and SFE characterization

Seven austenitic alloys, designated as alloys A–G, were selected for this study. The compositions of these alloys are shown in Table 1. Alloys B–G are solution annealed high purity alloys made by the General Electric Company. Alloy A is a commercial grade 304 stainless steel obtained from ABB Atom. Tensile samples with dimensions shown in Fig. 1 were fabricated by Shular Tools, TN. As a standard procedure for proton irradiations, the sample surfaces were mechanically polished to a fine grit of #4000 followed by electropolishing for 30 s in a 10% perchloric acid in 90% method solution at −40 °C. The electropolishing was necessary in order to produce surfaces free of damage caused by mechanical grinding prior to irradiation.

Several empirical correlations between SFE and composition were established in the literature [16–18]. The SFEs of the seven alloys estimated from two popular correlations by Pickering [16] and Rhodes [17] are listed in Table 1. The predicted SFE is useful as a guide, but it needs to be verified experimentally. The most straightforward method of measuring SFE in the austenitic alloy is to measure the separation of dislocation partials. In the face-centered cubic (fcc) structure, a perfect dislocation ($b = a/2\langle 1\,1\,0\rangle$) dissociates into two partial dislocations ($b = a/6\langle 1\,1\,2\rangle$) on {1 1 1} planes. The spacing of the two dislocation partials (d) at equilibrium is inversely proportional to stacking fault energy (γ) as given by [19]

$$d = Gb^2/4\pi\gamma \quad (1)$$

where G is the shear modulus and b is the Burgers vector.

SFEs of the alloys were measured using 3-mm TEM disks cut from each alloy and mechanically thinned to ~100 μm. They were then electropolished in a jet-thinner to produce a TEM foil. The TEM measurements of the spacing of dislocation partials were performed using a JOEL 2010F transmission electron microscopy (TEM) at the University of Michigan Electron Microbeam Analysis Laboratory (EMAL). Only isolated dislocations which are at least 100 nm away from others were selected for measurements. The selected dislocations were imaged using (g, 3g) weak beam dark field technique (WBDF) on {1 1 0} planes. At least 15 measurements were made on each alloy. Details of the technique will be published elsewhere [20].

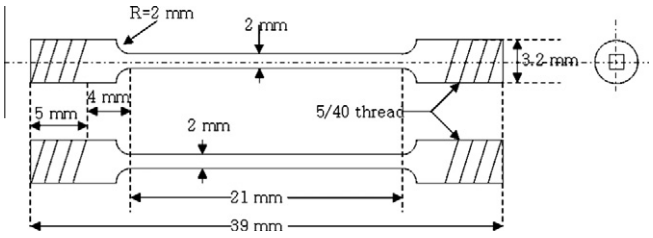

Fig. 1. Dimensions of the tensile sample.

2.2. Proton irradiations and hardness measurement

The irradiation experiments were conducted using 2 or 3.2 MeV protons in a Tandetron accelerator at the Michigan Ion Beam Laboratory (MIBL). Each alloy was irradiated to two doses of 1 and 5 dpa, respectively, at 360 °C. The sample temperature was monitored using a 2-dimensional thermal imager during each irradiation. The temperature variation was kept within ±10 °C by adjusting the amount of heating and cooling received from a heater and an air-cooling loop. A detailed description of the proton irradiation procedure was published elsewhere [21]. The dose rate was calculated to be $\sim 8 \times 10^{-6}$ dpa/s using the TRIM code [22]. Penetration depths were 25 μm for 2 MeV protons and 40 μm for 3.2 MeV protons.

Microhardness was measured using a Vickers hardness indenter (MICROMET II) with a load of 25 g. The low load confined the plastic zone ahead of the indenter tip to a depth within the proton range to ensure that unirradiated material was not being sampled. About 20 indents were made for each measurement.

2.3. Characterization of RIS

Radiation-induced segregation at grain boundaries was measured via STEM/EDS using either the JEOL 2010F at EMAL or the Philips CM200/FEG TEM–STEM at the Oak Ridge National Laboratory. EDS was done in the STEM mode in either of the microscopes. The electron beam was aligned by using the Ronchigram technique (JOEL 2010F) [23] or following standard alignment procedure on Philips CM200. The FWHM of the electron beam was ~1.5–2 nm. Prior to the measurement, the grain boundary was aligned edge-on to the electron beam. This can be done by minimizing the projected width of the grain boundary during sample tilting. 5–10 EDS line scans (15 points over 30 nm of length) across the grain boundary were performed and the intensities at each point were recorded. Under the very stable conditions when no sample drift was observed, electron beam was placed on the grain boundary and single spot collecting mode was used. The compositions were calculated using the k-factors that were obtained by matching the intensity ratio with the composition ratio of the bulk alloy. The k-factors related the ratio of measured intensities for a pair of elements to the ratio of compositions for the same pair of elements. Major elements such as Fe, Ni and Cr were analyzed. Minor

Table 1
Compositions (wt.%) and stacking fault energies of selected alloys. The SFEs were estimated using Pickering's [16] and Rhodes correlations [17]. NM means "not measured".

Alloy	Nominal	Fe	Cr	Ni	Mn	Si	P	C	SFE (mJ/m^2)	
									Pickering	Rhodes
A	18Cr8Ni	Bal.	18.30	8.50	1.38	0.65	0.03	0.04	25.2	19.5
B	18Cr12Ni	Bal.	17.49	11.87	0.98	0.11	0.014	0.02	39.3	40.7
C	15Cr12Ni	Bal.	15.76	12.04	0.98	0.10	<0.01	0.02	41.3	40.4
D	22Cr15Ni	Bal.	22.00	15.00	1.00	0.10	NM	0.02	42.9	53.1
E	13Cr15Ni	Bal.	13.41	15.04	1.03	0.10	<0.01	0.016	47.7	44.1
F	18Cr25Ni	Bal.	18.00	25.00	1.00	0.03	0.01	0.02	66.0	63.4
G	21Cr32Ni	Bal.	20.73	31.16	0.94	0.10	0.014	0.014	72.7	69.4

elements such as Si were only analysis in heat A because of its relatively higher content than other high purity alloys. Out of the three major elements, Cr concentration at the grain boundary was used in the correlation with IASCC as Cr was believed to be the most important element in IASCC.

2.4. Constant extension rate tensile (CERT) tests

Cracking susceptibility and localized deformation were evaluated using CERT tests. Cracking susceptibility experiments were carried out in a high temperature, high pressure autoclave under simulated BWR normal water chemistry (NWC) conditions consisting of 288 °C water containing dissolved oxygen (2 ppm) and a conductivity of 0.2 μS/cm at the outlet. The strain rate was 3.5×10^{-7}/s. To accommodate the range of susceptibilities of the alloys to cracking, samples were strained to 1% and 3%. Cracking initiated at very low strain and 3% was sufficient to determine if the alloy is susceptible to IASCC.

A set of straining experiments was conducted on a parallel set of samples in 288 °C argon for the purpose of measuring the degree of localized deformation at the same strain levels as for the cracking experiments. Although the cracks may be characterized on the samples tested in water, the oxide film covered the slip steps and made the characterization of localized deformation very difficult. The same strain rate and strain increments were used in the Ar tests as in the water tests.

2.5. Characterization of cracking susceptibility and localized deformation

Following CERT tests in water, cracks were characterized using scanning electron microscopy (SEM). The number of cracks and the crack length were quantified to determine the degree of susceptibility to IASCC. IASCC susceptibility can be determined in a number of ways. The most commonly used measures are the existence of cracks (whether cracks were observed for an alloy under a certain testing condition), crack number density (number of cracks initiated per unit area), crack length per unit area (the extent of cracking incorporating both the density and length of cracks), and percentage of cracking on the fracture surface with intergranular (%IG) character. The %IG was not characterized since samples were not taken to failure. However, the cracks on the samples are generally intergranular. Therefore, the existence of cracks, crack number density and crack length per unit area are the measures used to quantify the cracking susceptibility in this study.

The degree of localized deformation due to dislocation channeling can be quantified using the characteristics of the dislocation channels, such as spacing between channels, channel width and channel height. The channel height was selected as the figure of merit to quantify localized deformation because it is the quantity most representative of the amplification of strain in the channels. Further, deformation in and near grain boundaries has been linked to IGSCC in previous work [10,24] and since channels initiate and terminate at grain boundaries, the full amount of strain in a channel must be accommodated at the grain boundaries. The weighted channel height provides the best measure of the localization of strain in the microstructure. The weighted average channel height, which uses the channel height itself as the weighting factor, is defined as: [25].

$$\bar{h} = \frac{\sum_{i=1}^{n} h_i^2}{\sum_{i=1}^{n} h_i}, \tag{2}$$

where, h_i is the channel height of ith dislocation channel.

Channel height was characterized using the NanoScope IIIa-Phase Atomic Force Microscope. The resolution of the AFM with an EV scanner is less than 1 nm. However, the lateral resolution is affected by the scan area. The scanner can sample 512 points in both the X and Y directions. For a scan area of 10 μm × 10 μm, the lateral resolution is about 20 nm (10 μm/512). As the spacing between dislocation channels is generally a few micrometers, the scan area covers only a couple of dislocation channels. The width of the dislocation channels as imaged by TEM is generally less than 100 nm, therefore AFM would not reliably characterize the channel width even with this small area. Fortunately, the resolution in the Z direction (channel height) is not affected as much since there is no sampling issue. The resolution in channel height should be a few nm.

Due to the limitation of the AFM sample stage, the entire tensile sample cannot be accommodated. Therefore, the channel height was characterized using high resolution replicas. The replicas constitute a smaller specimen, which is better suited for AFM analysis and a durable archive of the specimen surface at each strain increment. The replicas were made using the Microset replica kits. Channel height measured from replicas was found to be slightly larger (a few percent) than the channel height measured directly from the sample surface. To be consistent, all the samples were characterized using the replicas.

Ideally, dislocation channels should be characterized in the grains under the same conditions (strain, orientation, etc.). Since identical conditions cannot be achieved, some criteria in selecting grains were established. Only grains of ~50 μm in size were selected. Grains with multiple sets of slip channels were rejected. Ten grains containing a total of 60–120 dislocation channels were characterized for each condition.

2.6. Correlation strength

IASCC follows a "threshold"-type of behavior in which cracking starts at a given dose in a particular environment [2] and becomes more severe with increasing dose until saturation occurs. As noted earlier, all of the features just described follow a similar dose dependence. Therefore, the dependence of IASCC on the value of the key feature should exhibit the same threshold-like behavior in which there is a regime of feature values that cause no cracking, followed by one in which the degree of cracking increases with the value of the feature. For real datasets, the way in which a particular feature, L, contributes to cracking will result in three regimes,

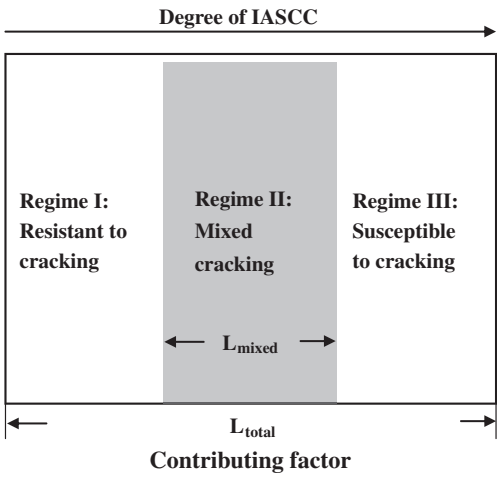

Fig. 2. Schematic showing the three regimes for a particular feature, L, that contributes to cracking. L_{total} is the total examined range of the feature and L_{mixed} is the portion of that range in which both cracked alloys and non-cracked alloys coexist.

Fig. 2. In regime I, there is no cracking for any value of L in that regime, while in regime III, cracking severity increases with the value of L. There will also exist a mixed cracking regime in which the feature fails to predict cracking susceptibility. That is, there is no relation between cracking severity and the value of L. Therefore, the wider is the mixed regime, the less important the feature is in correlating with cracking. If the mixed regime is very narrow (ideally, a single value), then the factor then is likely a predominant one. To distinguish the relative importance of each feature, its contribution to IASCC will be assessed using the correlation strength (S_{IASCC}), defined by:

$$S_{IASCC} = (L_{total} - L_{mixed})/L_{total}, \quad (3)$$

where L_{total} is the total examined range of a factor. It is calculated as the total range of the available data (the maximum value minus the minimum value). L_{mixed} is the range of the mixed cracking regime. The determination of L_{mixed} and L_{total} are shown in Fig. 2.

3. Results and discussion

3.1. SFE, hardness, RIS and weighted dislocation channel height

The results of SFE, hardness, RIS (Cr content at grain boundaries) and weighted dislocation channel height characterization that were published in [25] are summarized in Table 2. Fig. 3 shows the measured SFEs compared to those predicted by both Pickering's and Rhodes correlations. The measured values are generally smaller than the predicted ones. However, both the measured and predicted values follow the same trend. The SFE differences among alloys are typically as expected. Depending on the locations of the characterized dislocations in the TEM thin foil, the separation between partial dislocations may be affected by the surface force (worse if the dislocation is very close to the sample surface). Therefore, the accuracy of SFE characterization using this method is not ideal. However, if the error in measurement is systematic and applies to the entire examined alloys, the correlation between SFE and IASCC should be reasonably accurate.

Fig. 4 shows the comparison of hardness after irradiation to 1 and 5 dpa among the seven alloys. The hardness is heavily dependent on irradiation dose. Significant increase in hardness (~40%) was observed in all alloys irradiated to 5 dpa compared to 1 dpa. Hardness ranges from 206 kg/mm^2 in alloy D to 266 kg/mm^2 in alloy A for 1 dpa and from 301 kg/mm^2 in alloy C to 363 kg/mm^2 in alloy A. At 5 dpa, the hardness for alloys B–G is comparable. The commercial grade alloy A has the greatest hardness for both doses.

The grain boundary Cr content after irradiation ranges from 12.2 wt.% to 19.3 wt.% in all the characterized conditions (Table 2). It shows some degree of dependence on the bulk Cr content (Fig. 5). Alloy D has the highest bulk Cr content (22 wt.%) and also the highest grain boundary Cr content (19.3 wt.%) after irradiation to 5 dpa. The grain boundary Cr contents in alloy C and E are the lowest due to their low bulk Cr contents (15 wt.% and 13 wt.%, respectively). The higher-than-bulk Cr content at grain boundary of alloy A at 1 dpa is due to the initial enrichment of Cr prior to irradiation. The grain boundary Cr content decreases with dose and at 5 dpa the grain boundary Cr is lower than the bulk content by 2.3 wt.%. Alloy F and G have a larger degree of Cr depletion than other alloys. Alloy E, which has the lowest bulk Cr content, shows less depletion.

Fig. 6 shows the comparison of weighted average channel height among the seven alloys irradiated to 1 and 5 dpa and

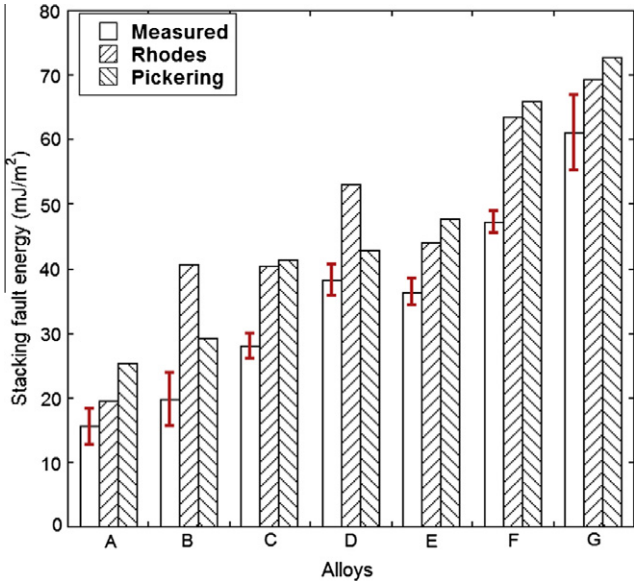

Fig. 3. Comparison of the measured SFEs (by partial dislocation method [19]) with the predicted values by Pickering's [16] and Rhodes' [17] correlation.

Table 2
Summary of the characterization results of stacking fault energy, hardness, RIS, cracking susceptibility and localized deformation following irradiation of alloys A–G to 1 and 5 dpa at 360°C. NM means "not measured".

Dose	Alloy	SFE (mJ/m^2)	Hardness (kg/mm^2)	RIS	Cracking susceptibility				Weighted Avg. Channel Height (nm)	
				Cr at G.B. (wt.%)	Number density (cm^2) at 1%	Number density (cm^2) at 3%	Length per unit area (μm/mm^2) 1%	Length per unit area (μm/mm^2) 3%	1% strain	3% strain
1 dpa	A	15.5	266.8 ± 14.5	18.8	0	20	0	3.6	197	311
	B	19.7	213.4 ± 12.5	NM	0	0	0	0	122	239
	C	28.0	231.9 ± 12.7	13.3	0	0	0	0	255	351
	D	38.2	206.4 ± 14.8	NM	0	0	0	0	NM	NM
	E	36.3	238.8 ± 12.2	12.3	0	0	0	0	190	288
	F	47.1	246.3 ± 9.4	NM	0	0	0	0	168	231
	G	61.1	243.7 ± 17.3	NM	0	0	0	0	119	180
5 dpa	A	15.5	363.0 ± 21.9	16.0	35	150	30	188	401	420
	B	19.7	314.5 ± 11.7	16.1	0	0	0	0	139	313
	C	28.0	301.3 ± 14.6	12.2	20	50	3.5	50.5	322	364
	D	38.2	321.3 ± 14.1	19.3	15	15	3.7	4.3	313	360
	E	36.3	327.9 ± 16.0	12.4	0	20	0	21.9	322	393
	F	47.1	329.8 ± 10.3	13.5	0	0	0	0	305	348
	G	61.1	338.3 ± 22.8	16.6	0	0	0	0	146	314

strained to 1% and 3%. Weighted average channel height varies among alloys. The biggest difference was observed between alloys C and G at 1 dpa and alloys A and B at 5 dpa. Irradiation dose promotes the channel height as it is always larger at 5 dpa at the same strain level, although the magnitude of the increase depends upon the alloy. Strain also promotes weighted average channel height, but the increase is minimal in alloy A irradiated to 5 dpa with the largest channel height, indicating that the channel height is likely approaching saturation in this alloy.

3.2. Cracking susceptibility

The total crack length per unit area and the crack number density observed on the irradiated surfaces are summarized in Table 2. The dependence of crack length per unit area on strain and irradiation dose is shown in Fig. 7. For all of the alloys irradiated to 1 dpa, cracks were only observed in alloy A. At 5 dpa, cracks were observed in alloys A, C and D at 1%. Cracks were also observed in alloy E at 3%. Alloys A and C showed the greatest degree of cracking susceptibility while alloys B, F and G showed no evidence of cracking of alloys D and E showed an intermediate degree of susceptibility. Both irradiation dose and strain promote cracking susceptibility, though the effect varies among alloy. Significant crack growth was found in alloys A and C when strained to 3% while there virtually no change in crack length in alloy D. Fig. 8 shows some typical SEM images of the cracked or uncracked surfaces of alloys A–G irradiated to 5 dpa and strained to 1 and 3%. All cracks appear to be intergranular in nature. In most cases, grain boundaries are highlighted by the dislocation channels as they generally start and terminate at grain boundaries.

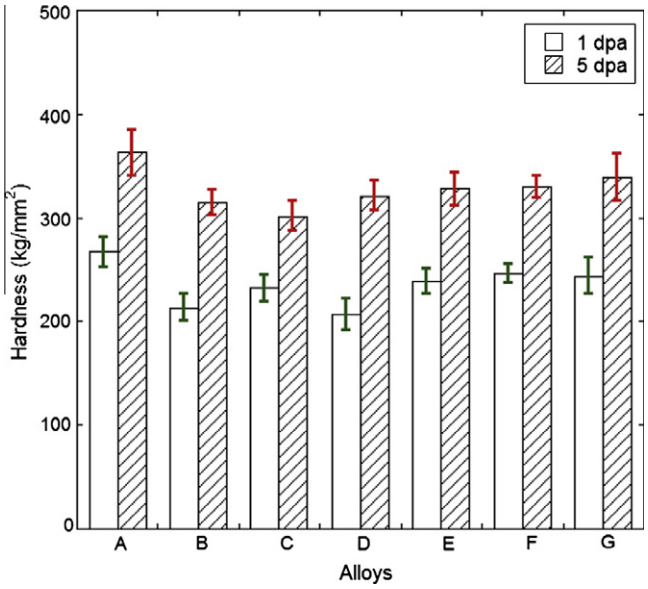

Fig. 4. Comparison of hardness among alloys after 1 and 5 dpa irradiation at 360 °C.

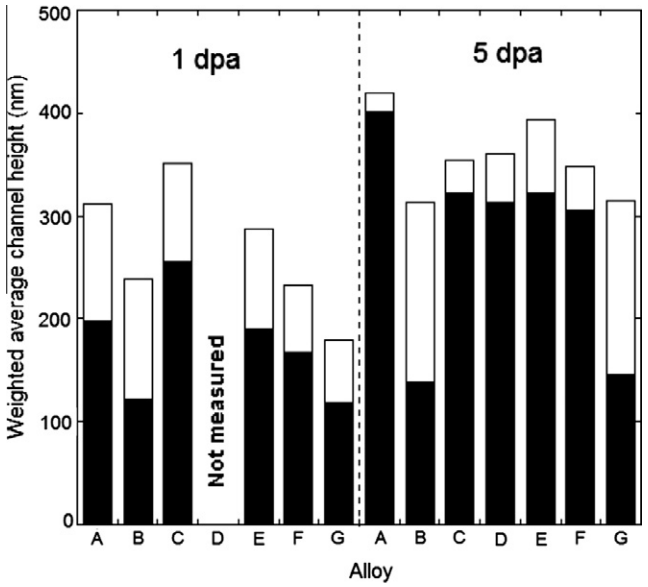

Fig. 6. Comparison of weighted average channel height of the seven alloys irradiated to 1 and 5 dpa. The height of each bar represents the weighted average channel height of the alloy strained to 3% at 288 °C with the solid portion representing that of the alloy strained to 1%.

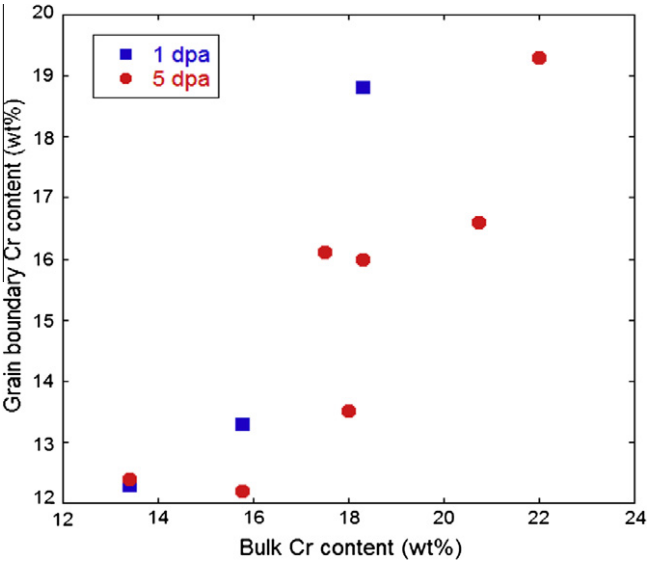

Fig. 5. Grain boundary Cr content as a function of the bulk Cr content in alloy A–G irradiated to 1 and 5 dpa at 360 °C.

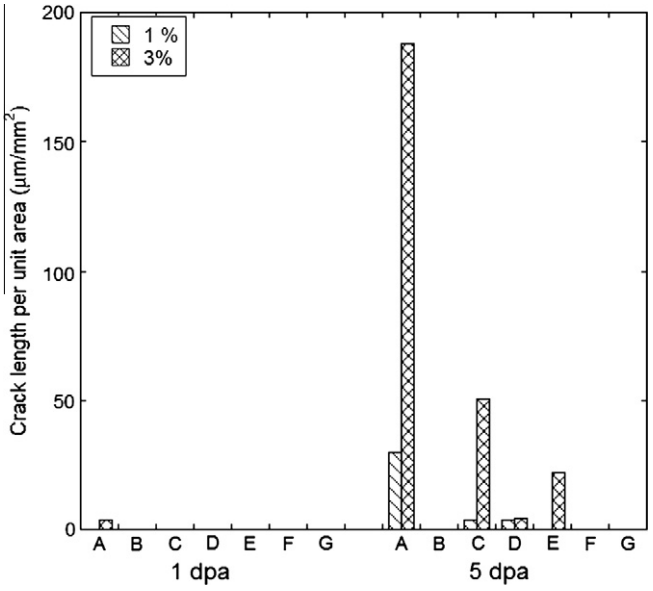

Fig. 7. Effect of irradiation dose and strain on crack length per unit area in alloys A–G irradiated at 360 °C and tested in simulated BWR environment at 288 °C.

3.3. Stacking fault energy and IASCC

The contribution of stacking fault energy to cracking is shown in Fig. 9, in which the cracking is characterized by the occurrence of crack initiation, crack number density and crack length per unit area.

The correlation strengths of SFE with IASCC are all around 0.5 (S_{IASCC}(SFE) = 0.5). This means that over the range of SFE examined (15.5–61.1 mJ/m^2), the cracking behavior cannot be predicted in half of that range (15.5–38.2 mJ/m^2). Careful examination of Fig. 9 shows that the two alloys (F and G) with SFEs higher than 38.2 mJ/m^2 are resistant to cracking.

The available literature data on the correlation between SFE and IASCC were also explored. Fig. 10 shows IASCC susceptibility as measured by %IG cracking as a function of stacking fault energy determined using Rhode's correlation for various data in [3]. The correlation strength of SFE with IASCC was calculated to be ~0.35. Alloys with high SFE (>50 mJ/m^2) are scarce due to the low SFE nature of austenitic stainless steels, but all of the data in this range showed resistance to cracking, which is consistent with results of this study.

Not surprisingly, the correlation strength does not change much whether it is calculated from crack initiation, crack number density or crack length per unit area. Nevertheless, from this point on, crack length per unit area will be used as the figure of merit to characterize the degree of IASCC because a yes/no criterion does not provide a "degree" of cracking, and crack density does not capture the length of the cracks.

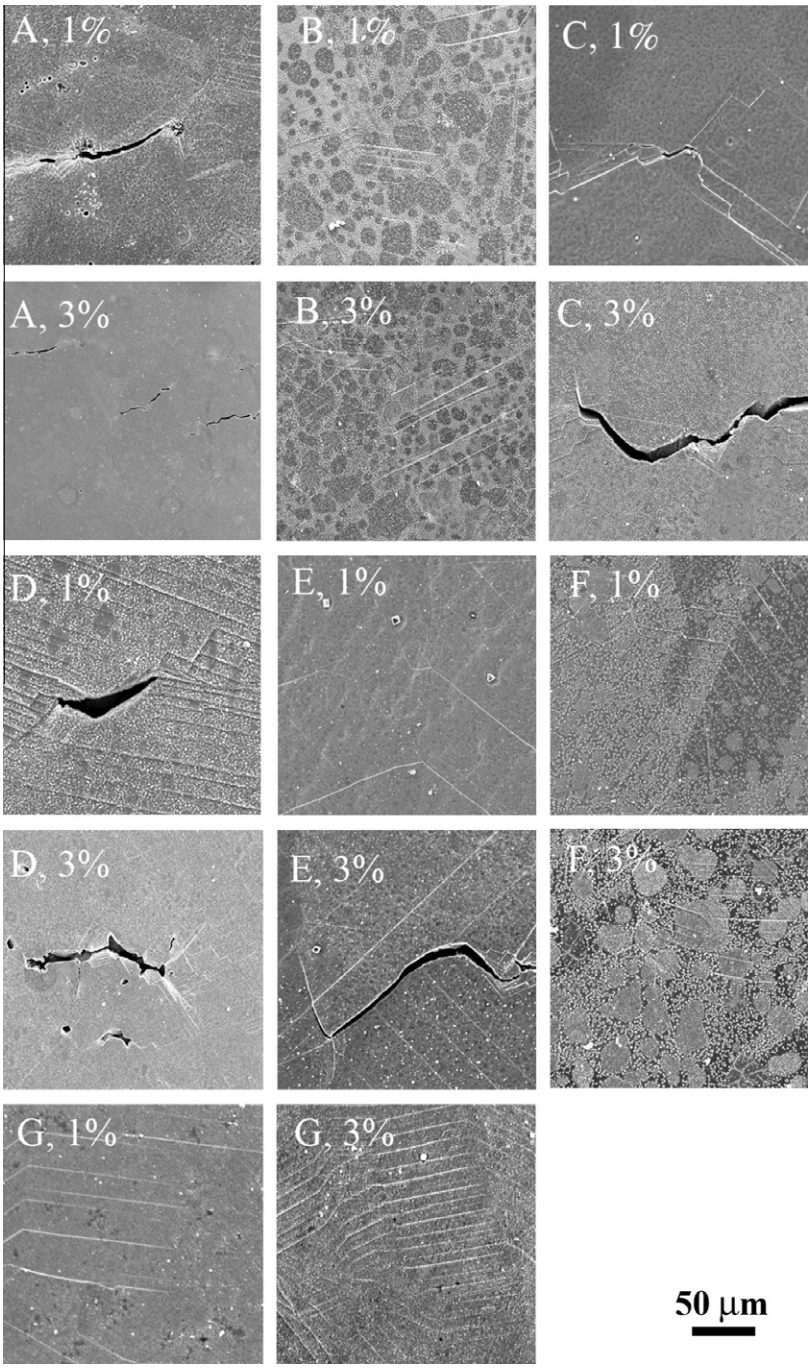

Fig. 8. SEM images of the irradiated surfaces after 1% and 3% strain for alloys A–G irradiated to 5 dpa at 360 °C.

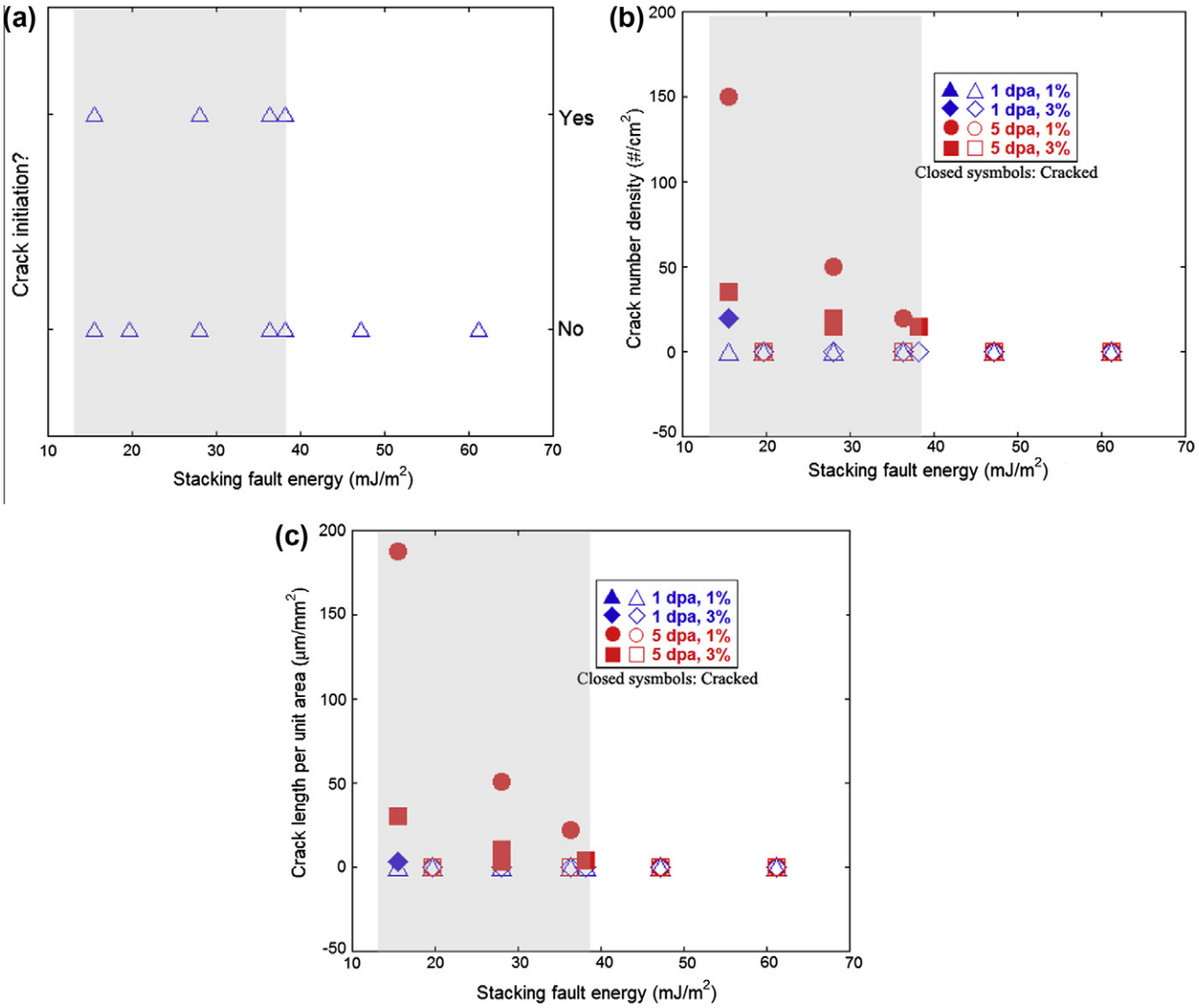

Fig. 9. The contribution of stacking fault energy to crack initiation (a), crack number density (b) and crack length per unit area (c). The correlation strength of stacking fault energy with IASCC, S_{IASCC}(SFE) = 0.5.

3.4. Hardness and IASCC

Fig. 11 shows the contribution of hardness to cracking susceptibility. The correlation strength of hardness with IASCC is 0.54 (S_{IASCC}(hardness) = 0.54). This value is close to that of SFE and IASCC, which was 0.5. The importance of hardness and SFE to IASCC is therefore of the same order. Alloys with hardness less than 250 kg/mm^2 are resistant to cracking. There is one single alloy (alloy A at 5 dpa) with the highest hardness that cracked at 1% strain. This suggests that only the extreme cases (very low or very high hardness) correlate well with IASCC. The majority of alloys with moderate hardness show no correlation with IASCC.

A similar trend was also observed from literature data. Fig. 12 shows the effect of yield strength on %IG in 300-series stainless steels. Alloys with yield strength less than 350 MPa are resistant to cracking while alloys with yield strength higher than 800 MPa are highly susceptible to cracking. The cracking behavior is mixed for alloys with yield strength between 350 and 800 MPa. The correlation strength of yield strength with IASCC is a ~0.5, which is consistent with the correlation of hardness with IASCC from this study.

Hardness is probably as important a factor as SFE in its contribution to IASCC. However, it failed to predict the cracking behavior of alloys with moderate hardness or yield strength. Recent post-irradiation annealing studies by Busby et al. [26] have also shown that hardening is not the primary cause of IASCC. Following post-irradiation annealing, IASCC susceptibility was removed before any change in hardening was measured. Therefore, hardening cannot be the primary cause for IASCC.

3.5. Radiation-induced segregation and IASCC

Fig. 13 shows the contribution of RIS (as measured using grain boundary Cr content after irradiation) to crack length per unit area. The correlation strength of RIS with IASCC (S_{IASCC}(RIS)) is zero. That is, there is no correlation of grain boundary Cr with cracking in the Cr range of 12–19 wt.%. Cracks were observed regardless of grain boundary Cr content. Since grain boundary Cr is believed to contribute to IASCC, it is unexpected to see that S_{IASCC}(RIS) = 0 in our study. Correlation strength was therefore examined using the data available from literature. Fig. 14 shows the effect of grain boundary Cr content on IGSCC for irradiated stainless steels complied in [3].

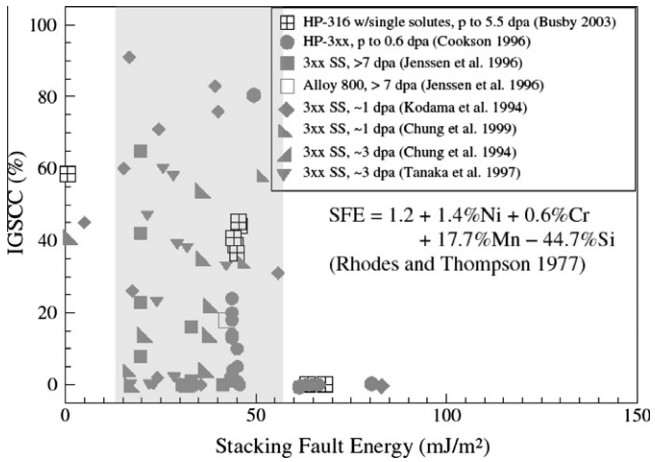

Fig. 10. IASCC susceptibility as measured by %IG cracking as a function of stacking fault energy determined using Rhode's correlation [3]. The correlation strength of stacking fault energy with IASCC, $S_{IASCC}(SFE) = \simeq 0.35$.

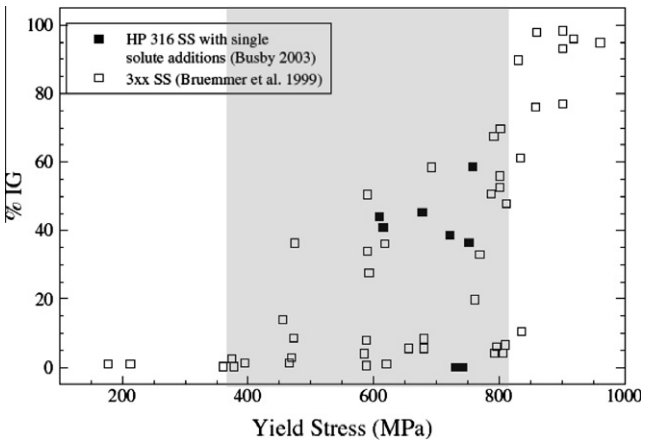

Fig. 12. Effect of yield strength on %IGSCC in 300-series stainless steels where hardening is by irradiation [3]. The correlation strength of hardness with IASCC, $S_{IASCC}(hardness) = 0.52$.

The correlation of grain boundary Cr with %IG was about 0.4. The grain boundary Cr was in the range of 10.5–21 wt.%. However, in the range of 12–19 wt.%, which is the range of our study, the cracking susceptibility is mixed. Actually, only alloys with grain boundary Cr less than 12 wt.% always crack. Above 12 wt.%, mixed cracking behavior was expected. Bruemmer and Was [27] suggested that grain boundary Cr content needs to be greater than 17 wt.% in order to gain the resistance to cracking. However, even grain boundary Cr contents above 17 wt.% did not guarantee that the alloy was resistant to cracking under LWR conditions. This can be seen from Fig. 14, alloys with high grain boundary Cr were still susceptible to cracking.

Post-irradiation experiments [26] also suggested that IASCC is relatively insensitive to RIS. The cracking susceptibility decreases significantly with annealing time while RIS remains unchanged. Therefore, RIS is not a predominant factor either. RIS may be the most important factor when the grain boundary Cr content is substantially low, say <12 wt.%, where localized corrosion may dominate IASCC.

3.6. Localized deformation and IASCC

The contribution of localized deformation to cracking susceptibility is shown in Fig. 15. As discussed in session 2.5, the weighted average channel height was used as a measure of the degree of localized deformation. The correlation strength of localized deformation with IASCC, $S_{IASCC}(LD) = 0.88$. It is the greatest among all the other examined factors ($S_{IASCC}(Hardness) = 0.54$, $S_{IASCC}(SFE) = 0.5$ and $S_{IASCC}(RIS) = 0–0.4$). The correlation of localized deformation with IASCC is also irrelevant to SFE, hardness or RIS. Fig. 16 shows the same graph as Fig. 15, but the SFE, hardness and RIS were identified and shown in three different categories (low, medium and high values). The data points indicated by arrows that are ill-predicted by other factors (high susceptibility to cracking according to other factors) fit well in the correlation of localized deformation with IASCC.

The formation of dislocation channels involves annihilation of irradiation defects by an array of dislocations [28] which are originated from grain boundary imperfections such as micro-scale ledges [29]. Irradiated microstructure, particularly dislocation loops, contributes most to the formation of dislocation channels.

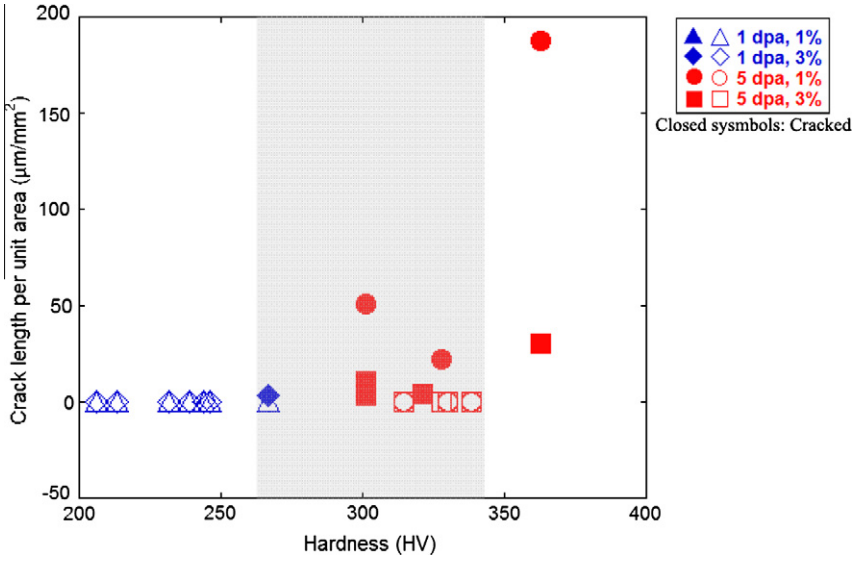

Fig. 11. The contribution of hardness to cracking susceptibility as measured using crack length per unit area. The correlation strength of hardness with IASCC, $S_{IASCC}(hardness) = 0.54$.

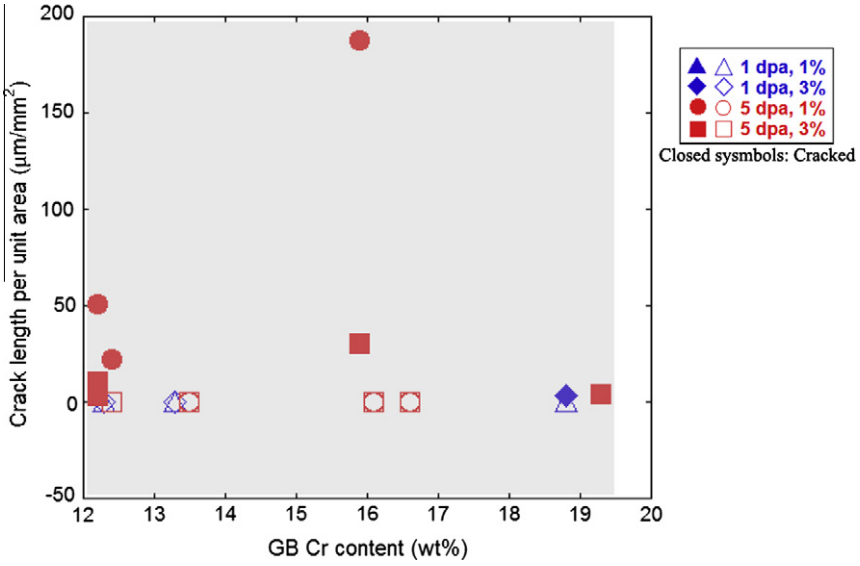

Fig. 13. The contribution of grain boundary Cr content to cracking susceptibility as measured using crack length per unit area. The correlation strength of grain boundary Cr content with IASCC, $S_{IASCC}(RIS) = 0$.

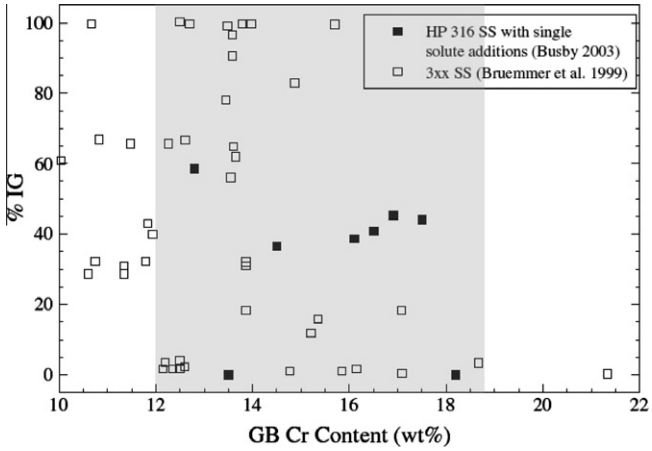

Fig. 14. Effect of grain boundary chromium content on IGSCC for irradiated stainless steels [3]. The correlation strength of grain boundary Cr content with IASCC, $S_{IASCC}(RIS) = 0.4$.

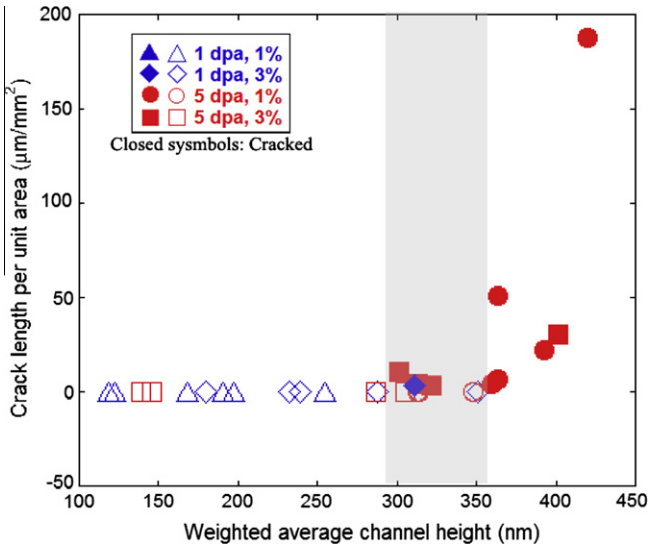

Fig. 15. The contribution of localized deformation as measured by the weighted average channel height to cracking. The correlation strength of localized deformation with IASCC, $S_{IASCC}(LD) = 0.88$.

[30] Once the dislocation channels are formed, dislocations are confined in the channels because the dislocation channels have much fewer obstacles than the surrounding matrix. When the dislocation channels transmit or terminate at the grain boundary, the dislocations in the channels will eventually impact on the grain boundary. The magnitude of the impact is likely to correlate to the total number of dislocations in the channels. Since the channel height is proportional to the number of glide dislocations in the channels, larger dislocation channels are likely to have larger impact on the grain boundary. This impact includes localized deformation near and in the grain boundary. The deformation near the grain boundary is less important in IASCC [10]. However, the deformation in the grain boundary, which is localized in the small portion of the grain boundary near the intersection of the dislocation channels and the grain boundary (referred to "localized grain boundary sliding" in [10]) could be linked to crack initiation.

As cracking was not observed in the same alloys in the parallel straining experiments in argon, localized deformation itself does not lead to IG cracking. In the argon environment, slip channels interact with grain boundaries and leave steps/ledges in the grain boundary [12]. While in the corrosive environment such as simulated BWR environment, they may cause crack initiation at grain boundaries with high cracking susceptibility (i.e. random high angle boundaries, inclination at a favorable angle (nearly normal to the tensile axis)). One difference between these two environments is that in the argon environment, step/ledge height increases continually as more and more dislocations interact with the grain boundaries. However, in the simulated BWR environment, the oxide film covers the grain boundary. Due to this oxide film barrier, a certain number of dislocations are needed to build up sufficient stress/strain in order to break the oxide film. As hypothesized in [3], the breakage of the oxide film is necessary for crack initiation and at the same time, larger dislocation channels are more efficient in pumping out large number of dislocations to advance the crack.

A certain amount of localized deformation is essential in order to break the oxide film that covers the grain boundary. The strong correlation between localized deformation and IASCC shown by

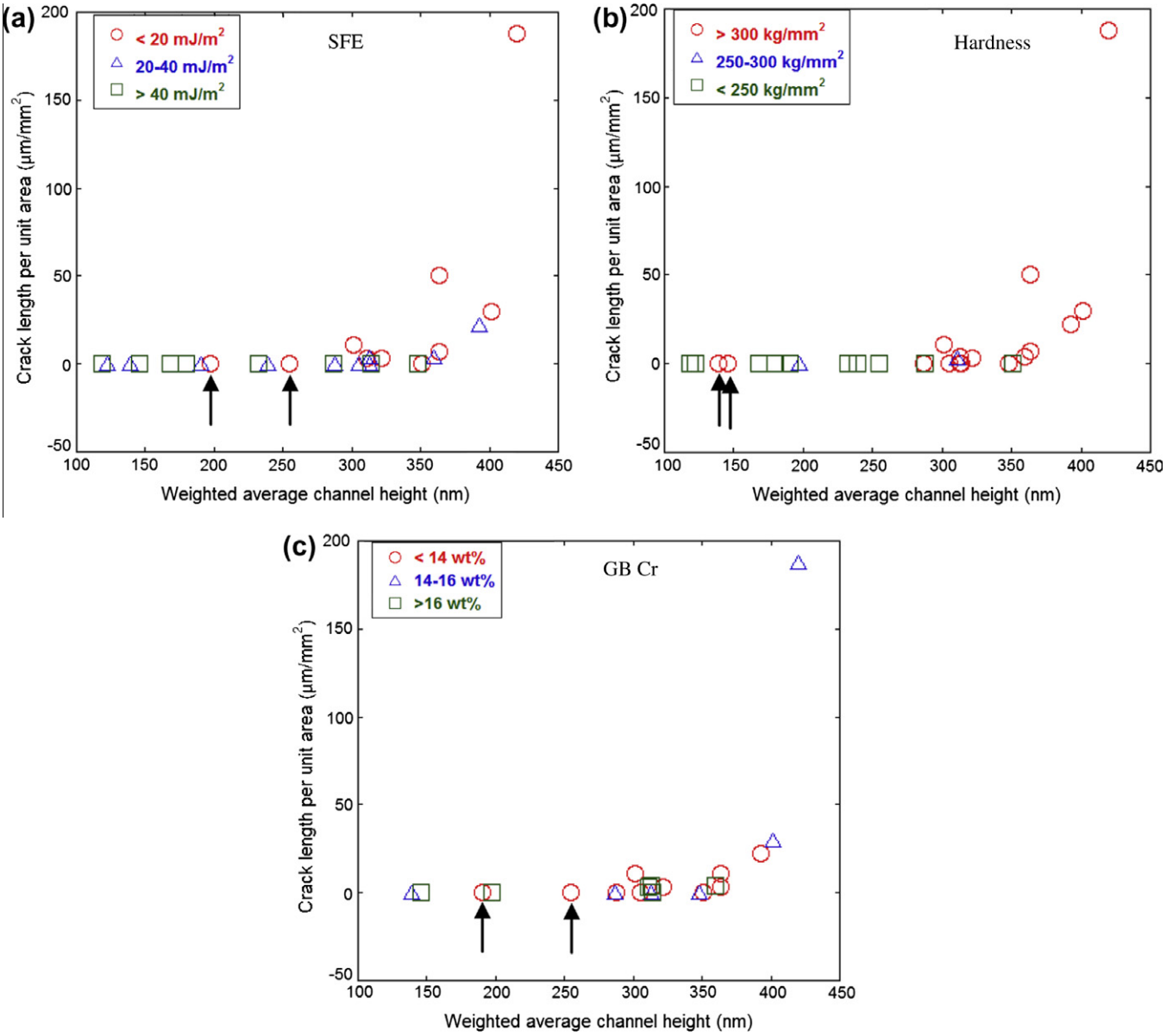

Fig. 16. The contribution of localized deformation to IASCC irrelevant to: (a) SFE, (b) hardness and (c) grain boundary Cr content. The data points indicated by the arrows are predicted to be susceptible to cracking by low SFE, high hardness or low grain boundary Cr content but they are resistant to cracking due to low degree of localized deformation.

this study underscores the importance of localized deformation in the IASCC process. A strong correlation between localized deformation and IASCC, however, does not, by itself, constitute a cause-and-effect relationship between localized deformation and IASCC. A cause-and-effect relationship needs to be established to verify that localized deformation is, indeed, responsible for IASCC. Further, a mechanistic description of how localized deformation leads to IASCC must also be established.

3.7. Interdependency of factors

It is worth noting that factors that influence IASCC are not completely independent of each other. For instance, slip planarity (localized deformation) in unirradiated fcc metals is affected by SFE and irradiation dose. The influence of SFE on slip planarity is expected to be less important once dislocation channels are formed in irradiated austenitic alloys as dislocation slip is constrained in the dislocation channels. However, for alloys with extremes in SFE such as alloys A and G, SFE may still be a key factor that affects the degree of localized deformation at low fluences. Yield strength as well as hardness may also influence localized deformation by affecting the separation between partial dislocations [31]. While SFE and hardness play a secondary role in IASCC, they may contribute to IASCC by enhancing the degree of localized deformation, which plays the primary role.

4. Conclusion

Seven austenitic alloys were irradiated to 1 or 5 dpa and tested both in simulated BWR NWC water and in argon at 288 °C. Cracking susceptibility as measured by crack initiation, crack density and crack length per unit area was evaluated at both 1% and 3% strain intervals. Alloy A was found to be the most susceptible to cracking for both 1 and 5 dpa. Alloys B, F and G were found to be resistant to cracking in simulated BWR environment.

In order to explain the differences in cracking behavior, factors such as SFE, hardness, RIS and localized deformation were characterized and their correlation with the degree of cracking were evaluated using the correlation strength. The correlation strengths of SFE and hardness with cracking were both around 0.5, indicating that both contributed to cracking but neither was the dominant factor. The correlation strength of RIS with cracking was zero in the grain boundary Cr content range of 12–19 wt.%. RIS did not play an apparent role in this study. The correlation strength of localized deformation, which was characterized using the weighted average channel height, with IASCC was found to be 0.88, which was significantly higher than others, implying that localized deformation may be the most important factor in IASCC of irradiated alloys in BWR environments. Localized deformation may promote cracking through intensive interaction of dislocations in slip channels with grain boundaries.

Acknowledgements

The authors gratefully acknowledge Drs. Ovidiu Toader and Fabian Naab for their assistance in conducting proton irradiations, Peter Andresen at the General Electric for making various heats of the alloys. The authors also acknowledge the facilities provided by the Michigan Ion Beam Laboratory and the Electron Microbeam Analysis Laboratory at University of Michigan. Support for this research was provided by EPRI under contract EP-P20763/C10134 and the Department of Energy (DOE) under contract DE-FG07-05ID14703. A portion of this research was conducted at the SHaRE User Facility, which is sponsored by the Division of Scientific User Facilities, Office of Basic Energy Sciences, US Department of Energy.

References

[1] P.L. Andresen, F.P. Ford, S.M. Murphy, J.M. Perks, in: Proc. Fourth Int'l Symp. On Environmental Degradation of Materials in Nuclear Power Systems – Water Reactors, NACE, 1990, pp. 1–83 to 1–121.
[2] G.S. Was, P.L. Andresen, Corrosion 63 (2007) 19.
[3] G.S. Was, J.T. Busby, Philos Mag 85 (2005) 443.
[4] A.W. McReynolds, W. Augustiniak, M. McKewon, D.B. Rosenblatt, Phys. Rev. 98 (1955) 418.
[5] T.H. Blewitt, R.R. Coltman, R.E. Jamison, J.K. Redman, J. Nucl. Mater. 2 (1960) 277.
[6] S.M. Bruemmer, E.P. Simonen, P.M. Scott, P.L. Andresen, G.S. Was, J.L. Nelson, J. Nucl. Mater. 274 (1999) 299–314.
[7] M.O. Speidel, R. Magdowski, In Ninth International Symposium on Environmental Degradation of Materials in Nuclear Power Systems—Water Reactors, in: F.P. Ford, S.M. Bruemmer, G.S. Was (Eds.), Metallurgical Society of AIME, Warrendale, PA, 1999, pp. 325–329.
[8] Y.V. Konobeev, S.I. Rudnev, At. Energy 53 (2) (1982) 107–108.
[9] S.M. Bruemmer, J.I. Cole, J.L. Brimhall, R.D. Carter, G.S. Was, in: Proc. Sixth Int'l Symp. on Environmental Degradation of Materials in Nuclear Power Systems - Water Reactors, TMS, 1993, p. 537.
[10] Z. Jiao, G.S. Was, J. Nucl. Mater. 382 (2008) 203.
[11] M.C. Hash, J.T. Busby, G.S. Was, in: Proceedings of the 21st International Symposium on Effects of Radiation on Material, ASTM STP 1447, M.R. Grossbeck, T.R. Allen, R.G. Lott, et al. (Eds.), American Society for Testing of Materials, West Conshohocken, PA, 2004, pp. 92–104.
[12] Z. Jiao, J.T. Busby, R. Obata, and G.S. Was, in: Proc. 12th International Conference on Degradation of Materials in Nuclear Power Systems – Water Reactors, The Minerals, Metals and Materials Society, Warrendale, PA, 2005, p. 379.
[13] Z. Jiao, J.T. Busby, G.S. Was, J. Nucl. Mater. 361 (2007) 218.
[14] T. Onchi, K. Dohi, N. Soneda, J.R. Cowan, R.J. Scowen, M.L. Castano, J. Nucl. Mater. 320 (2003) 194.
[15] T. Onchi, K. Dohi a, N. Soneda, Marta Navas, M.L. Castano, J. Nucl. Mater. 340 (2005) 219.
[16] F.B. Pickering, in: Proceedings of the Conference on Stainless Steels 84, Gothenberg, Sweden, 1984, The Institute of Metals, London, 1985, p.2.
[17] C.G. Rhodes, A.W. Thompson, Metal. Trans. A 8A (1977) 901.
[18] R.E. Schramm, R.P. Reed, Metal. Trans. A 6A (1975) 1345.
[19] D. Hull, D.J. Bacon, Introduction to Dislocations, International Series on Materials Science and Technology, vol. 37, Pergamon Press, 1984. p. 98.
[20] Z. Jiao, J.T. Busby, G.S. Was, Metall. Mater. Trans. Commun. In preparation.
[21] G. Gupta, Z. Jiao, A.N. Ham, J.T. Busby, G.S. Was, J. Nucl. Mater. 351 (2006) 162.
[22] J.F. Ziegler, J.P. Biersack, SRIM2003 program, IBM Corp., Yorktown, NY, 2003.
[23] J.M. Rodenburg, E.B. Macak, Microsc. Anal. 90 (2002) 5–7.
[24] B. Alexandreanu, G.S. Was, Corrosion 59 (2003) 705.
[25] Z. Jiao, G.S. Was, J. Nucl. Mater. 407 (1) (2010) 34–43.
[26] J.T. Busby, G.S. Was, E.A. Kenik, J. Nucl. Mater. 302 (2002) 20.
[27] S.M. Bruemmer, G.S. Was, J. Nucl. Mater. 216 (1994) 348.
[28] T.S. Byun, N. Hashimoto, J. Nucl. Mater. 354 (2006) 123.
[29] I.M. Robertson, A. Beaudoin, K. Al-Fadhalah, Li. Chun-Ming, J. Robach, B.D. Wirth, A. Arsenlis, D. Ahnc, P. Sofronis, Mater. Sci. Eng. A 400–401 (2005) 245–250.
[30] A. Luft, Prog. Mater. Sci. 35 (1991) 97.
[31] T.S. Byun, Acta Mater. 51 (2003) 3063.